Simulation and Analysis of Opportunistic MSPA for Multiple Cubesat Deployments

Zaid J. Towfic, David P. Heckman, David D. Morabito, Ryan M. Rogalin, Clayton M. Okino, and Douglas S. Abraham
Jet Propulsion Laboratory, California Institute of Technology, Pasadena, California, 91109

We describe a software approach for simultaneous demodulation and decoding of multiple frequency- multiplexed spacecraft across multiple ground stations. The approach involves the use of a single ground antenna with wide enough aperture to receive multiple angularly adjacent spacecraft simultaneously. This technique uses a wide-band RF signal digitizer coupled with easily and cheaply duplicated software-receiver modules to independently process the frequency-channelized downlink signals from the spacecraft. This approach relaxes the need for realizable modems at each antenna, for example in the Deep-Space-Network (DSN), and can also function as a delayed data retrieval method for cubesat missions with routine science data return. Thus, we hope that this solution can enable more efficient utilization of DSN assets.

We concentrate on a simulation similar to the proposed *Exploration Mission 1* (EM-1) mission from a geometric perspective. To that end, the simulated scenario involves ten secondary cubesats deployed and tracked for a span of four days (the modeled motion over the first four days of the mission does not include any Trajectory Correction Maneuvers (TCMs) that may be necessary as the cubesats approach the moon). Transmissions from the cubesats may be received through a combination of DSN ground sites based on visibility. The cubesats are assumed to utilize typical cubesat transmit powers and a waveform similar to that of the Iris radio. One cubesat is chosen as the "target" and is considered tracked by all ground-stations throughout the simulation (i.e., it is consistently at the center of the main lobe of each ground station antenna when the ground station is in view of the cubesat in terms of elevation angle). The simulation effort involves synthesizing a wideband signal that includes the ten cubesats across a large bandwidth due to each cubesat having its own center-frequency in X-band, near 8.4 GHz. Each signal is characterized by its own Doppler-frequency shift and free-space path-loss computed through the underlying geometry of the simulation as well as the cubesat transmit power. Finally, each cubesat signal experiences a unique antenna gain at each ground station due to the underlying antenna pattern and spacecraft-ground station geometry.

We establish two interesting findings: First, the link-budget for the EM-1-like scenario is almost completely limited by the angle between the center of the antenna main beam and the cubesat, which means that the signal-to-noise ratio is wholly adequate for demodulation and decoding at the simulated bitrates unless the cubesat exits the main beam. Secondly, and fortunately due to the use of a software radio architecture, we show that it is possible to successfully receive signals from most cubesats for the entire 4-day simulation. Due to the signal-to-noise ratio being sufficient for demodulation even after the side-lobe's 17dB reduction in SNR, the software radio can still demodulate such cubesats as long as the radio is capable of re-establishing carrier lock as the cubesats leave the main beam and enter the side-lobe. Considering that the target application utilizes offline processing, a loss of lock can be detected and lock can be re-established by iterating over the data. Extensive simulations demonstrate these results.

I. Introduction

Between now and 2027, the number of spacecraft relying on the Deep Space Network (DSN) for communications is projected to double. While the DSN is building new 34m beam-waveguide antennas that can be arrayed to back up some of its aging 70m antennas and can be used in lieu of the old 34m High Efficiency Feed (HEF) antennas that are being retired, the net total number of antennas will only increase by two—from 13 antennas today to 15 antennas in 2024. Since the rate at which new antennas are being built cannot be expected to keep pace with the anticipated increase in the number of DSN-supported spacecraft, NASA's Space Communications and Navigation Office (SCAN) is having the DSN pursue a three-pronged strategy for accommodating the growing demand. This strategy includes: (1) developing ways to use a single antenna to simultaneously support multiple spacecraft, (2) establishing cross-support arrangements with other space agencies, universities, and other entities that possess deep-space-capable antennas, and (3) developing spacecraft navigation techniques that are less reliant on traditional radiometric data, potentially reducing the overall amount of two-way tracking required.

The first prong in this strategy, using a single antenna to simultaneously support multiple spacecraft, is the overall category of activity to which this paper relates. For well over a decade, the DSN has made use of a technique called Multiple Spacecraft Per Antenna, or MSPA. In this technique, missions that determine that their spacecraft will be within the half-power beam-width of a single antenna, can schedule to share the antenna such that their downlinks will simultaneously come down through the same antenna to separately assigned receivers. In the past, this technique has been limited by the number of available receivers, and the scheduling system, to just two spacecraft (2-MSPA). While the two spacecraft can simultaneously share the downlink, there is not yet a way for multiple spacecraft to simultaneously uplink through the same transmitter. So, the two spacecraft have had to share the uplink in a serial fashion, with the first spacecraft up-linking for the first half of the pass, and the second spacecraft up-linking for the second half of the pass. Recently, the DSN has extended its MSPA capability to simultaneous downlink support for four spacecraft, or 4-MSPA. It has done this by making additional receivers available to a single antenna and adjusting the scheduling system accordingly. For uplink, each spacecraft transmits for roughly a quarter of the total downlink pass duration (minus calibration time between each spacecraft), sharing it in a serial fashion. The DSN's current analog IF distribution architecture makes moving beyond 4-MSPA cost prohibitive. However, it is pursuing a new common platform architecture in which digitization occurs at each antenna, rather than at each Complex's signal processing center—making it easier to replicate the IF streams and redirect them to any number of much cheaper, software-based receivers. Hence, in the not-too-distant future, the DSN hopes to have a schedulable n-MSPA capability. This report, however, focuses on a fundamentally different type of MSPA technique, Opportunistic MSPA (OMSPA).

Instead of relying on an antenna's receivers, OMSPA relies on a wideband recorder that captures (from the down-converted IF) whatever the antenna "sees" in the frequency range of interest. So, if we had several cubesats, for instance, that determined they would be within the half-power beam-width of an antenna for which some other mission has already scheduled a traditional downlink, they could arrange to opportunistically transmit open loop during that timeframe. If a wideband recorder was active for that antenna during the timeframe, the open loop transmissions would be captured on the recorder. The cubesat missions could then retrieve the time- and frequency-relevant portion of the recording, demodulate and decode the signal on it, and recover their data—or subscribe to a service that would do it for them. To the extent that each of the cubesat users abide by the appropriate process for obtaining a frequency assignment, there would be virtually no limit to how many in-beam users could make use of the technique. In reality, of course, the number of users would be limited by the available recorder bandwidth. But, this number would generally be greater than that for 4-MSPA and, in the common platform era, would likely scale more economically than the number of receivers inherent to n-MSPA. More, importantly, however, OMSPA users would not have to formally schedule their downlinks in the DSN's scheduling system. Instead, they would just have to figure out when they would be in-beam with some other mission that does have a formally scheduled downlink or uplink and transmit open-loop (given that there is a recorder actively capturing everything the antenna is "seeing"). Because the OMSPA users would not have to schedule an antenna and would not be at frequencies that would interfere with those that do (or with each other), they would not compete for antenna time—thereby reducing the amount of antenna scheduling conflicts that all users would otherwise see. OMSPA users would essentially be "invisible" to the scheduled user community. In an era where the number of DSN users is likely to double, this could prove very useful.

OMSPA is not without its limitations, however. The most obvious is that the simultaneous users have to be within the half-power beam-width of the same antenna. Only at Venus, Mars, and more distant destinations is this almost always the case for DSN antennas. For closer destinations, such as at the Moon, the beam intercept conditions and duration have to be carefully calculated. There are also circumstances where a constellation or flotilla of spacecraft may remain together within the beam-width of a single antenna for a protracted time period. In such cases, one of the

spacecraft can have a formally scheduled downlink and/or uplink while the other spacecraft can make opportunistic use of the scheduled beam for their downlinks.

A second limitation has to do with the fact that it is a downlink-only technique. Unlike regular MSPA, there is no serial sharing of the uplink over the course of the pass. Up-linking requires a scheduled antenna pass. So, OMSPA would not be a useful technique when commanding and/or two-way radio-metrics for navigation are required.

A third limitation is latency. It takes more time to retrieve a recording, demodulate it, decode it, and recover the data than it takes a traditional receiver to demodulate and decode "on the fly." So, OMSPA is not a technique one would want to rely upon for receiving time-critical data.

Limitations aside, however, OMSPA may be a viable technique for recovering routine science data when operating in-beam with one or more other spacecraft that have a scheduled downlink or uplink. Since the OMSPA user would not schedule an antenna, presumably they would incur fees lower than the current antenna aperture fees—perhaps only some sort of small flat-rate fee in support of the OMSPA recorder and user interface infrastructure. While NASA missions do not actually pay DSN antenna aperture fees, these fees do figure prominently in their "bottom line" during their proposal phase. So, keeping the amount of such fees to a minimum would still be in the missions' best interest. For non-NASA reimbursable missions, antenna aperture fees actually have to be paid. Hence, keeping such fees as low as possible would definitely be in the missions' best interest.

In the case of mission-critical events, OMSPA could also be useful as a backup to a traditional scheduled downlink, if executed via a separate in-beam antenna. That way if, for some reason, the telemetry on the scheduled downlink was not immediately recoverable, the mission could then attempt to recover its data from the OMSPA recording made on the other in-beam antenna. The total cost to the mission (at least in the proposal phase) would likely be less than if scheduling both a primary antenna and a backup antenna.

Given OMSPA's potential benefits, SCaN funded the DSN to undertake an initial demonstration of the technique during FY 2014. The demonstration involved obtaining Mars Odyssey's telemetry via a VLBI Science Receiver (VSR) recording made from an antenna that was capturing the Mars Reconnaissance Orbiter's traditionally scheduled downlink. Known as "Opportunistic MSPA Demonstration #1," the test was executed three times[1]—once from each Complex. Recording playback times from the Complexes to JPL Central and across the flight projects firewall to a prototype OMSPA Software Demodulator (OSD) were carefully documented and ranged from 2 h 16 min to 10 h 34 min for 1 h worth of Mars Odyssey data (~14.4 GB). The time to demodulate, decode, and recover the data in each case was also carefully recorded and generally ran from 5 to 6 times longer than the recorded duration. Validation of the recovered data was accomplished by comparing the transfer frames obtained through OMSPA with those recovered via Mars Odyssey's formally scheduled downlink. In most cases, 100% of the recorded data was recovered. In the worst-case demonstration pass, 11 out of 23,624 frames exhibited unresolvable errors—equivalent to 99.95% successful data return. The demonstration observed somewhat long recording playback times that subsequent investigation revealed to be due to a VSR data prioritization issue in the DSN's ground communications lines and a fundamental playback rate limitation in the decades-old VSR itself. In addition, the demodulation times could have been accelerated with multi-core processing. However, the demonstration results strongly suggested that OMSPA could be successfully applied to the routine science downlink needs of low-bandwidth missions (e.g., cubesats) within reasonable timeframes (i.e., less than a day). An Interplanetary Network Progress Report detailing the demonstration and its results is available[1].

In FY 2017, SCaN funded two OMSPA follow-on demonstrations: one applying OMSPA to the provision of backup telemetry during the near-simultaneous deployment of multiple cubesats from a launch vehicle upper stage (Opportunistic MSPA Demonstration #2) and one applying OMSPA to the simultaneous capture of downlink data from multiple Mars spacecraft (Opportunistic MSPA Demonstration #3). Since there have not yet been any deep space cubesats deployed from a launch vehicle's upper stage, Opportunistic MSPA Demonstration #2 was necessarily conducted as a simulation. The simulation was loosely modeled on the then-projected October 2018 launch of Exploration Mission One (EM-1) and the 10 or more cubesats that might be deployed from the upper stage of its launch vehicle. The purpose was to show that the downlink signals from ten cubesats that were released in groups of four or so near-simultaneous deployments, if captured during the same recording, could be individually acquired, demodulated, decoded, and the data recovered within a reasonable amount of time and with high accuracy—thereby showing OMSPA to be a potentially viable backup to the scheduled downlink support for EM-1-like cubesat deployments.

In this paper, we report the results of this EM-1-like simulation. The simulation assumed 10 cubesats are launched in small groups from the Space Launch System's upper stage (called the Interim Cryogenic Propulsion Stage, or ICPS) and travel toward the moon on an ICPS-like trajectory. The group launch events are referred to as "bus stops." In the study, a single cubesat was modeled as being 'tracked' and was always treated as 'in-beam', in the center of the main antenna beam. All the other cubesats were modeled as being opportunistically received. The cubesat

deployments from the ICPS were modeled according to parameters that were determined from recent Space Launch System design documents, with a few assumptions made to fill-in undetermined information and provide a system of complete cubesat motion models.

Related studies were conducted, before the present ones, to explore the expected behaviors of groups of non-maneuvering cubesats launched from SLS upper stages during lunar missions. It was found that the gravity gradients near the moon can cause groups of cubesats to spread apart rapidly after a lunar flyby. Figure 1 shows a lunar flyby typical of the case studied here, with the associated spreading of cubesats during the event.

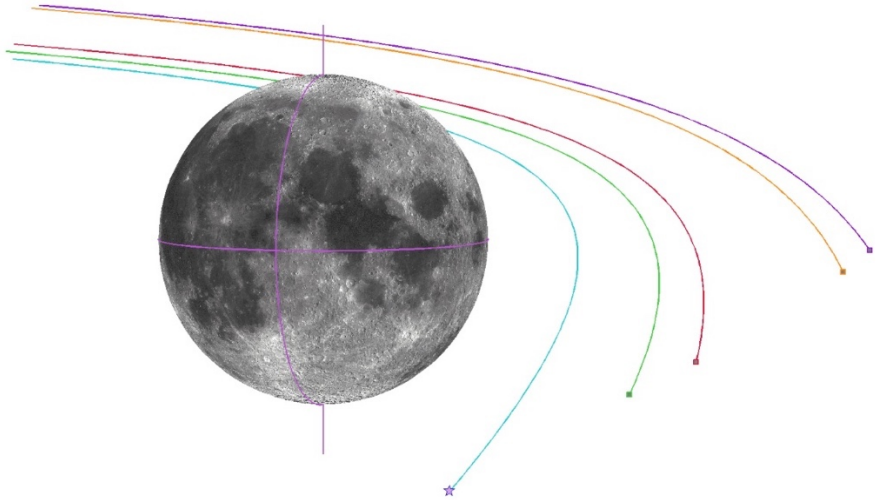

Figure 1: The ICPS (star marker) and four cubesats in a typical lunar flyby. Cubesat clusters are usually greatly spread apart by the lunar flyby, but it is a delicate phenomenon that varies significantly with cubesat launch parameters.

This gravitational effect tends to move non-maneuvering objects too far apart for a group of them to be kept in-beam much past a lunar flyby. Lacking knowledge of any particular hypothetical cubesat's maneuvering plans or specific cubesat trajectory file(s), this study was conducted under the assumption that cubesats , once launched from the ICPS, do no maneuvering for the duration of the analysis, that being 4 days (96 hours.) The duration of 4 days was chosen to avoid the lunar flyby event that would occur shortly thereafter, in accordance with a 2017 ICPS design reference trajectory. As an aside, an earlier study demonstrated that if cubesats were released *after* the lunar flyby, the gravitational environment then allows them to typically remain in-beam for many days.

II. Link-budget Overview

To study the benefits of opportunistic MSPA, we will first consider the link-budget for near-earth missions such as EM-1-like scenarios. To do this, we may compute the effective received power at the receive antenna on earth via (all quantities in Equation (1) are in Decibel):

$$P_{\text{received}} = P_{\text{EIRP}} - PL + G_{\text{Earth}} \qquad (1)$$

where P_{EIRP} denotes the Effective Isotropic Radiated Power (EIRP), which we treat to be the actual transmit power out of the transmission chain combined with the spacecraft antenna gain in the direction of the Earth antenna (essentially, it is the power out of the spacecraft antenna in the direction of the receive antenna on Earth). Additionally, PL denotes the total pathloss between the spacecraft antenna and the receive antenna. This value is mainly dependent on the distance between the spacecraft and Earth, the frequency at which the transmission occurs, and the speed of the electromegnatic wave through the medium (which we assume to be the speed-of-light in a vacuum):

$$PL = 20\, log_{10}\left(\frac{4\,\pi\, d\, f}{c}\right)$$

where d denotes the distance between the spacecraft and the receive antenna, f denotes the carrier frequency, and c denotes the speed-of-light. Finally, the Earth antenna gain denoted by G_{Earth} will also be an influential factor in the link-budget calculation. As we will see, the beam-width of this antenna will have a big impact on whether the total receive power is sufficient for demodulation. For simplicity, we ignore media loss such as due to atmosphere.

First, we assumed that a reasonable transmit EIRP of cubesats under consideration is around 10 dBW. Clearly, there are some cubesats that may far exceed this value, but for our purposes, we believe that a value on the lower end of the spectrum of EIRPs suffices to provide a pessimistic estimate of performance of the system.

Secondly, the path-loss can be estimated using the distance between the moon and the Earth (clearly, during a scenario such as EM-1, the distance steadily grows as the cubesats approach the moon). Using a frequency of 8.4 GHz (X-band), the path-loss is approximately:

$$PL = 20\log_{10}\left(\frac{4\pi \cdot 384.4\times 10^{6}\cdot 8.4\times 10^{9}}{2.998\times 10^{8}}\right) \approx 222.629\ \text{dB}$$

Finally, if the cubesat is being tracked, the expected receive antenna gain at a 34-m antenna is approximately 68.2 dB at X-band[2]. This means that the total received power at the receiver (excluding other minor losses) is given by:

$$\begin{aligned} P_{\text{received}} &\approx P_{\text{EIRP}} - PL + G_{\text{antenna}} \\ &= 10\ \text{dBW} - 222.629\ \text{dB} + 68.2\ \text{dB} \\ &= -144.429\ \text{dBW} \\ &= -114.429\ \text{dBm} \end{aligned}$$

This is typically sufficient for demodulation purposes as received powers needed for moderate bitrates are around -140 dBm (lower levels are receivable at lower bit rates). For example, the "DSN NOW" website lists a downlink signal from *2001 Mars Odyssey* being received at -135.26 dBm and the link operating at a data rate of 14.22 kbps. It is emphasized that this case assumes a very small contribution of hotbody noise from Mars. For the case of cubesats crossing near or on the disk of the moon, the hotbody contribution to system noise temperature needs to be considered.

In the next section, we will focus on the receive antenna gain term G_{antenna}, which will not be a constant in the *Opportunistic* MSPA scenario since the cubesats will be distributed across the antenna beam as opposed to all being concentrated at the center of the beam.

III. Impact of Antenna Size

In the typical MSPA scenario, a single spacecraft is chosen to be "tracked," meaning that the antenna is pointing towards one spacecraft, and if another spacecraft happens to appear within the beamwidth of the antenna, then the second spacecraft can be received so long as its frequency is not overlapping. That is, multiple spacecraft can be received simultaneously assuming they are using different frequency channels via frequency division multiple access (FDMA). Still, the antenna affects the MSPA aspect by two main attributes:

- The Antenna Gain
- The Antenna Beamwidth (half-power beamwidth or null-to-null beamwidth)

Both of these aspects are directly affected by the antenna size: a larger antenna yields a higher gain but a smaller beamwidth. Figure 2 illustrates this direct relationship between the antenna diameter and gain and inverse relationship between antenna diameter and null-to-null beamwidth. For this reason, the MSPA scenario holds a trade-off: a larger antenna will have higher gain, but the main beam will be narrower.

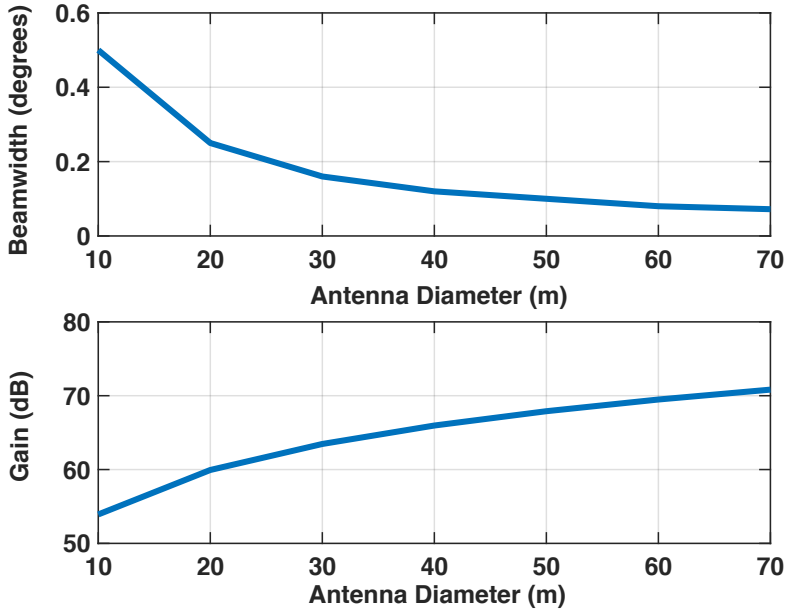

Figure 2: Illustration of antenna gain in decibels and null-to-null antenna beamwidth (degrees) vs the antenna diameter in meters at 8.4GHz.

IV. ICPS and Cubesat Trajectory Models

To model the motions of a group of cubesats, it was first necessary to model the motion of their launch platform, the ICPS. This was accomplished by using a very precise initial time and associated orbital state vector supplied by personnel at Marshall Space Flight Center and by integrating the trajectory forward in time from that information. The orbital model corresponded to a launch date of EM-1 on 2018 OCT 07 with an ICPS transit of about 5.7 days to closest lunar approach. After the lunar flyby, the ICPS leaves the Earth-Moon system permanently, going into an Earth-like solar orbit. Integration of the ICPS trajectory and those of the cubesats was done using point mass gravity from the Earth, Moon, and the Sun and solved using a high quality solar system ephemeris.

With the basic motion of the cubesats' launch platform modeled, several other parameters were still required before any representative models of cubesat trajectories could be generated. For example, the evolving orientation of the ICPS during its motion, the locations of cubesats inside the ICPS prior to their launches, and the timing of each cubesat launch from the ICPS were all parameters that must be set before cubesat trajectories could be inferred. Much of this information was obtained from Marshall Space Flight Center, spread over a few different documents. In particular, the cubesat launch sequence and angular positions within the ICPS fairing were specified in the detailed diagram in Figure 3, with the planned deployment sequence indicated by the boxed numerals.

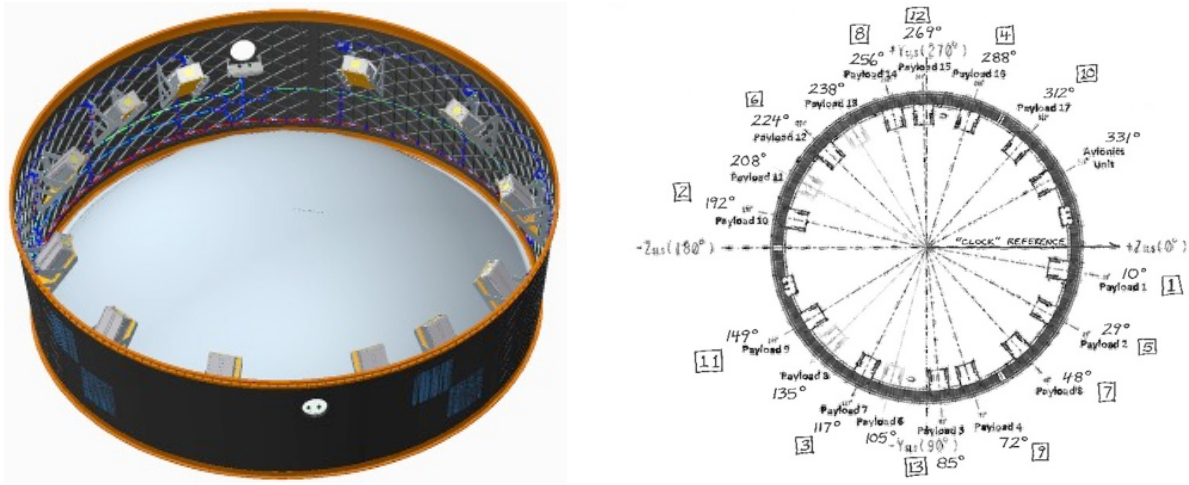

Figure 3: A rendering of the ICPS adapter ring (left) and the adapter ring's payload positions and planned release sequence, with the sequence given by the boxed numerals (right.) The diagrams were supplied by Marshall Space Flight Center with hand edits added.

Other parameters required for modeling cubesat motions included:

- Axial "barbecue" roll motion parameters for the ICPS.
- Dimensions of the ICPS and deployer tilt angles of the stowed cubesats in the ICPS fairing ring.
- Cubesat launch times during the ICPS flight, using the "bus stop" model of frequent launches in separate small groups.
- Cubesat launch speeds off the spring-loaded deployer units in the ICPS fairing (set at 1.5 m/s).

Our study hypothesized a set of 10 cubesats in total, with 6 launched in the first group and 4 in the second group. Each group was set to launch at a plausible bus stop event, as outlined in MSFC documents, and within each group, all cubesats were treated as being launched with 20-second temporal spacing. The 6th cubesat launched, which is the last one in the first group, was treated as the tracked host for aligning the antenna line-of-sight from each ground station, and all other cubesats were treated as being opportunistically received.

V. Overview of DSN and DSN-Affiliated Antennas

The DSN antennas examined in this study were the 34-meter diameter antennas. These antennas are located in Canberra, Australia, Madrid, Spain, and Goldstone, California and assumed to have a gain of 65 dB. The DSN-Affiliated antenna, a 21-meter antenna, located in Morehead, Kentucky was assumed to have a gain of 60 dB. The 21-meter antenna, while having a smaller gain, has a much larger beam-width. Meaning it is more likely that the entire cubesat constellation would remain inside of the main beam for the duration of the simulation (4 days). Figure 4

illustrates the normalized antenna patterns for the 34-m and 21-m antennas, respectively. Observe that the 34-m antenna has a beamwidth (mainbeam) of 0.14 degrees null-to-null (the half-power beamwidth of the 34-m antenna at X-band is 0.066 degrees during downlink). On the other hand, the 21-m antenna has a beamwidth of 0.24 degrees null-to-null. Clearly, the smaller antenna has a beamwidth advantage.

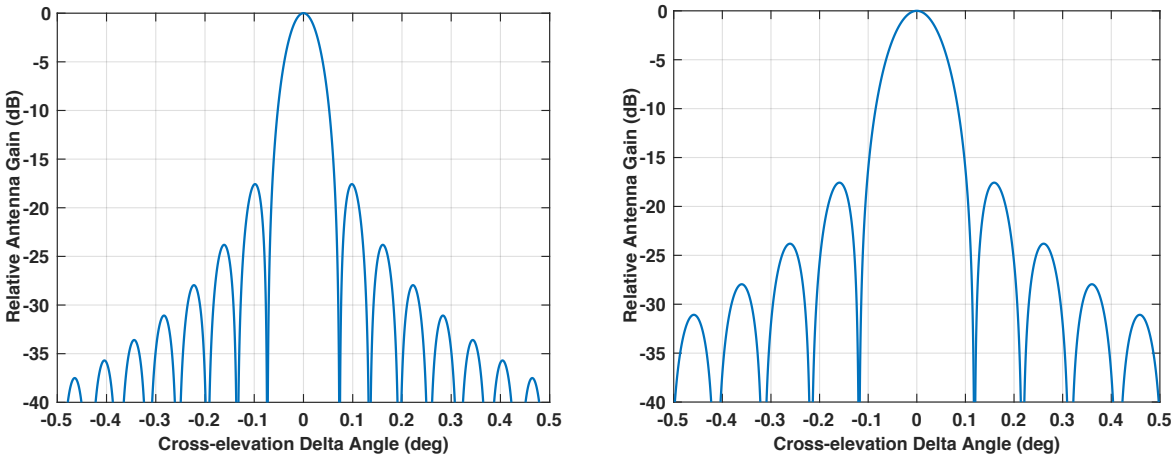

Figure 4: Comparison of antenna patterns for 34m (left) and 21m (right) antennas.

We will later show through simulations that the use of large antennas like the 21m and 34m antennas provide adequate gain for the lunar-bound deployment scenarios. For this reason, even if the spacecraft signal is received through a sidelobe, the antenna gain through the sidelobe may still be sufficient for the decoder.

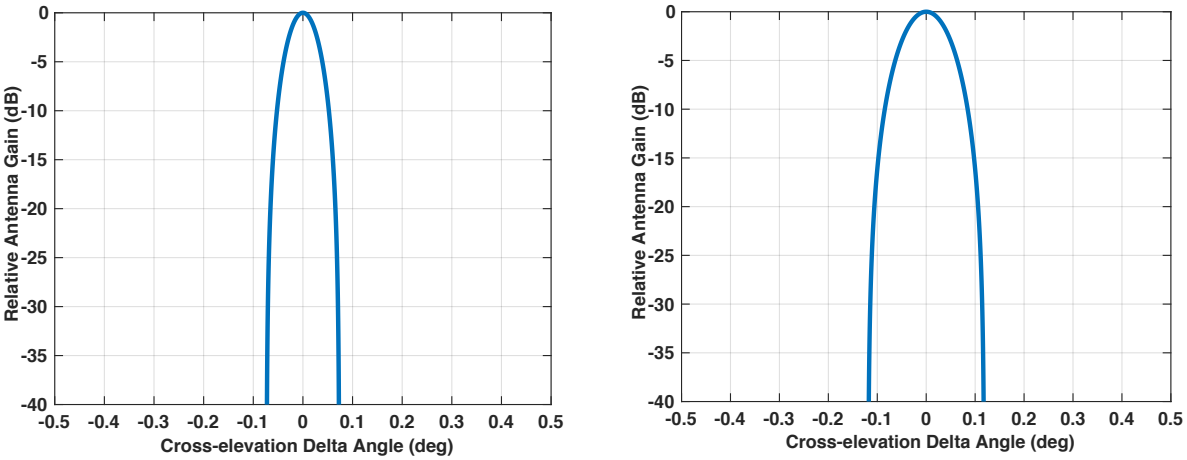

Figure 5: Comparison of antenna patterns for 34m (left) and 21m (right) antennas with no sidelobes.

We assume that a ground-site has no visibility of the cubesat constellation when the elevation angle of the constellation is lower than 7 degrees. This means that it is necessary to switch to receiving the data from another ground station. Figure 6 illustrates the coverage of the ground stations Canberra, Madrid, Goldstone, and Morehead for the simulated cubesat constellation. Observe that the constellation is always visible from at least one ground station based solely on elevation angle (this figure does not take power into account).

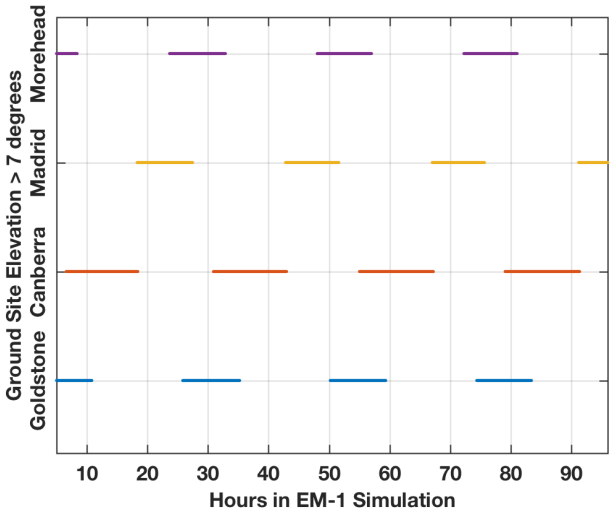

Figure 6: Visibility of cubesat constellation from the ground sites Canberra, Madrid, Goldstone, and Morehead. If a marker is present, then the constellation is visible at the ground site.

VI. Receiver Architecture

In this section, we examine two major receiver architectures, illustrated in Figure 7:

1. Channelizing Hardware Receiver/Digitizer
2. Wideband Hardware Receiver/Digitizer

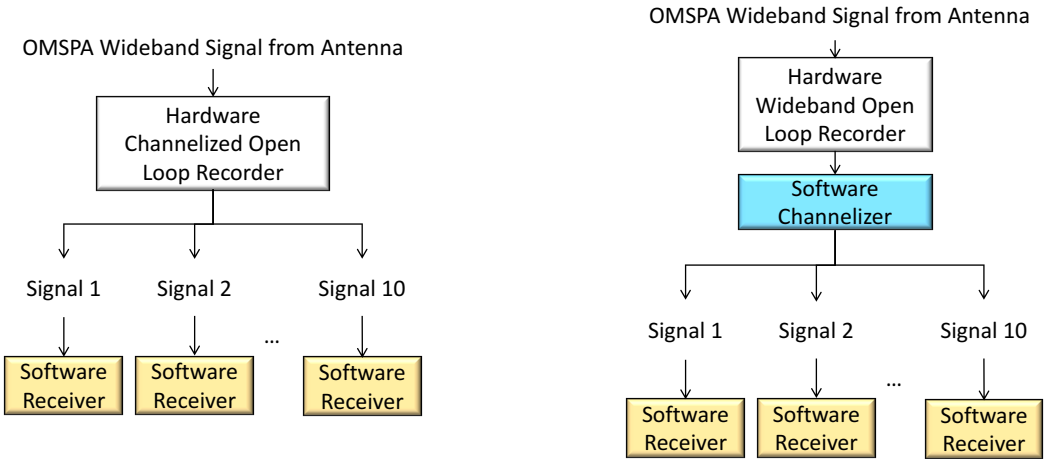

Figure 7: Receiver Architectures: The hardware architecture (left) collects 10 "narrowband" RF channels, which can each be processed by the software receiver. The software architecture (right) collects a single "wideband" RF channel, which needs to be channelized in software to yield 10 narrower-band baseband signals.

The main difference between the two architectures is that the former architecture performs the frequency channelization in hardware, while the latter relies on the software receiver to perform the frequency channelization. While either method is acceptable from an OMSPA perspective, it is preferable for the digitizer to perform the channelization in general since the output channelized file sizes will be smaller due to the smaller per-channel bandwidth and thus easier to transfer. In addition, the software-receiver processing chain requires per-sample processing including:

- Reading the samples from the file.
- Signal Acquisition
- Timing Recovery

The complexity of these steps are proportional to the bandwidth of the input signal. For these reasons, a channelizing digitizer is greatly favored for OMSPA application. With this in mind, however, both architectures are theoretically equivalent.

VII. Simulation Architecture

The simulation architecture follows that of the wideband receiver architecture in Figure 7, meaning that the signals were generated for the ten cubesats at different frequencies. The cubesats were placed randomly in a spectrum spanning 85MHz and centered at a frequency of 8428.6MHz. For the waveform itself, a recorded file of a CCSDS modem without a carrier was used. The recording was done through a laboratory test and the waveform was recorded in lab with a symbol-rate of 48000 symbols/seconds and BPSK modulation with a code rate of 1/6 (i.e., the information rate is 8 kbps). The signal was Manchester coded (as opposed to NRZ). The data was Turbo coded and it included a cyclic-redundancy-check (CRC) block. Different cubesats were assigned random sections of the laboratory recording for their transmission waveform so that no two cubesats "transmitted" the same signal. Since the initial signal was obtained by sampling the output of a radio, the SNR was effectively extremely high and treated as infinite. Each incoming waveform with high SNR was shifted in frequency and scaled based on the received power at the antenna. The received power at the antenna has three significant components, as discussed earlier in Equation (1):

- Pathloss
- Ground Antenna Gain
- EIRP

Following the scaling of the clean CCSDS signal, a frequency shift was introduced to account for the Doppler shift induced at the cubesats in addition to the CCSDS signals being shifted according to their assigned frequency. These signals were then added together in addition to the receiver noise according to:

$$r(t) = n(t) + \sum_{k=1}^{N} s_k(t) e^{j2\pi(f_{CS,k} - f_c + f_{d,k})t}$$

where $r(t)$ is the modeled received signal, $s_k(t)$ is the clean signal of cubesat k, $f_{CS,k}$ is the cubesat k frequency in Hertz, f_c is the receiver center frequency in Hertz, and $f_{d,k}$ is the Doppler shift frequency of the k-th cubesat relative to the receiver in Hertz. Finally, $n(t)$ denotes the receiver noise. A noise temperature of 33.5K was utilized in the simulation[2]. This simulation architecture is illustrated in Figure 8.

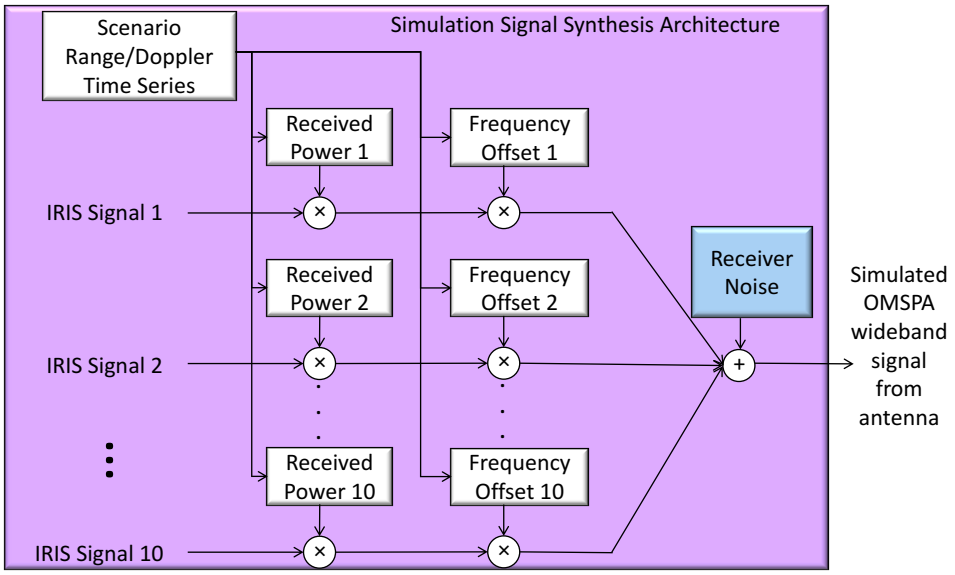

Figure 8: Simulation synthesis architecture.

Following the synthesis of the wideband signal, it was necessary to simulate the wideband receiver architecture that involves channelization of the wide bandwidth. To do this, the wideband signal $r(t)$ was passed through a frequency down-conversion stage followed by a low-pass filter to isolate cubesat k-th signal plus noise from the other cubesat signals. This architecture is illustrated in Figure 9.

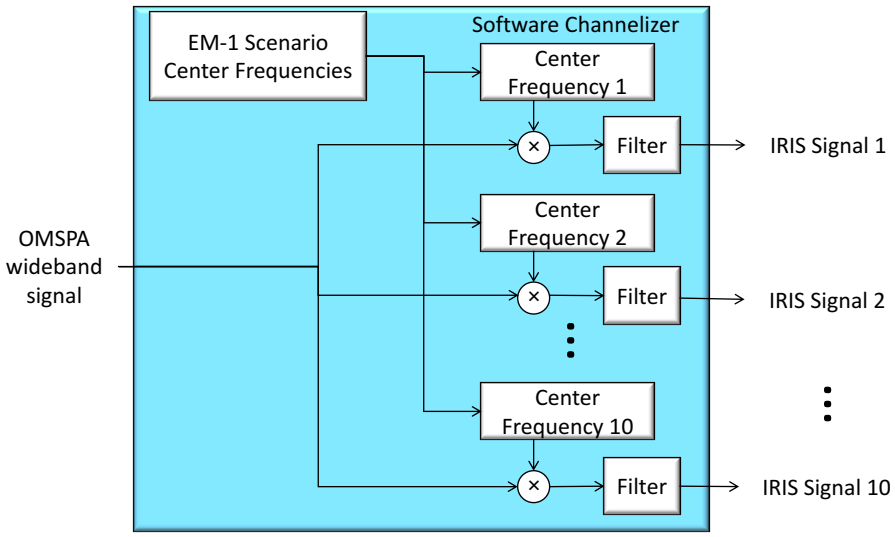

Figure 9: Simulation channelization architecture.

Finally, each down-converted and filtered signal was demodulated and decoded. This was done via the software receiver architecture as outlined in a previous publication[3]. The structure of this software receiver is illustrated in Figure 10. The software receiver involved the detection of the frequency shift induced by the receiver circuitry as well as the Doppler shift due to the cubesat trajectory. Following this, the symbol timing was detected and tracked and the soft symbols were extracted and correlated against the Attached Synchronization Marker (ASM). This was followed by running the extracted time-aligned soft symbols through the decoder to extract the desired databits as well as the cyclic-redundancy-check (CRC) block. This CRC block was then used to verify the successful decoding of the data frame.

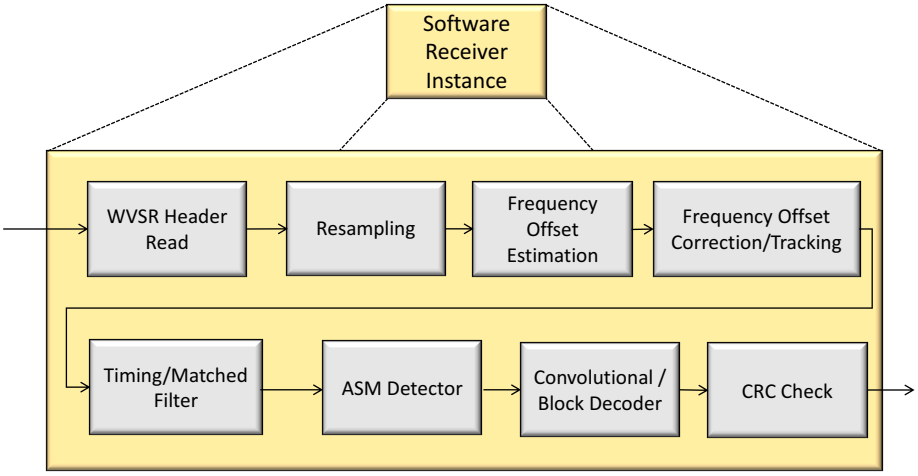

Figure 10: Software receiver architecture

VIII. Results

As the cubesat constellation moved through the sky in the simulation, different ground stations were tasked to track it (by tracking the designated cubesat in the constellation). In this section, we present the results for not using sidelobes; i.e., the antenna pattern was assumed to only contain the main lobe, as illustrated in

Figure 5. The results of the simulations are illustrated in Figure 11. We observe that six out of the ten total cubesats will experience bit-error-rate less than 1E-3 (uncoded) and seven out of the ten cubesats will experience an out of decoder bit-error-rate of less than 1E-6 (decoded). For the three cubesats that failed to meet the 1E-6 decoded BER for the duration of the simulation, it can be seen that they achieved this metric for almost 60 hours. However, there were some brief periods where these three cubesats can exit the main beam and not be able to close the link. As these cubesats exit the main beam, the antenna gain becomes too low for the decoder to be able to correct the errors.

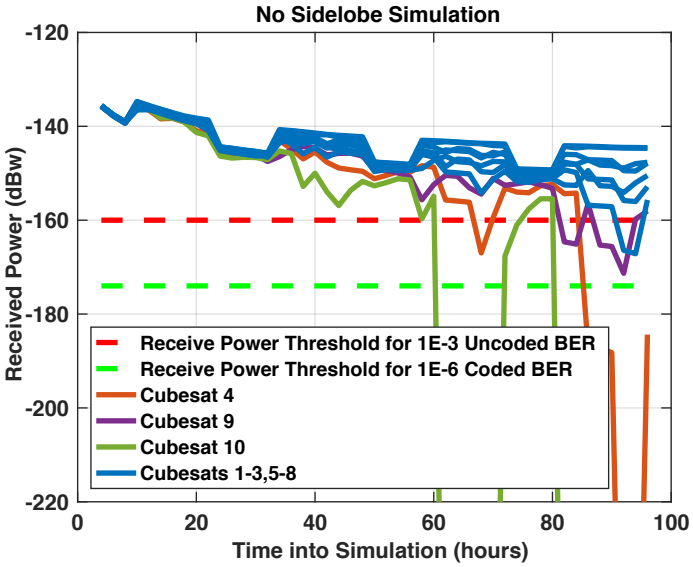

Figure 11: Simulation result with no use of side-lobes. Observe that six out of the ten total cubesats will experience bit-error-rate less than 1E-3 (uncoded) and seven out of the ten will experience bit-error-rate less than 1E-6 (decoded). The simulation sampled the time-line every 2 hours for the 96-hour simulation duration. The three cubesats (4, 9, and 10) experience significant bit errors due to them leaving the main beam of the receive antenna during their trajectory, which in turn causes the receive power of the signal to drop too low to be successfully demodulated and decoded.

Unfortunately, due to the complexity of the simulation, the results were obtained every two hours during the entire simulation time-line of 96 hours. For this reason, another simulation method was performed to get a more finely sampled result. The alternative did not require the synthesis and channelization of a wide-band signal but assumed that no SNR degradation occurs at those stages (which should be true in a well designed down-conversion chain). Instead, we performed the time-consuming software-receiver simulation only once, but at different receive powers in order to plot the bit-error-rate (BER) before and after decoding. The result of this was the BER vs. received power illustrated in Figure 12. It is easy to see that the coded bit-rate curve is very sharp and the steep drop-off occurs around -174dBw, which is expected.

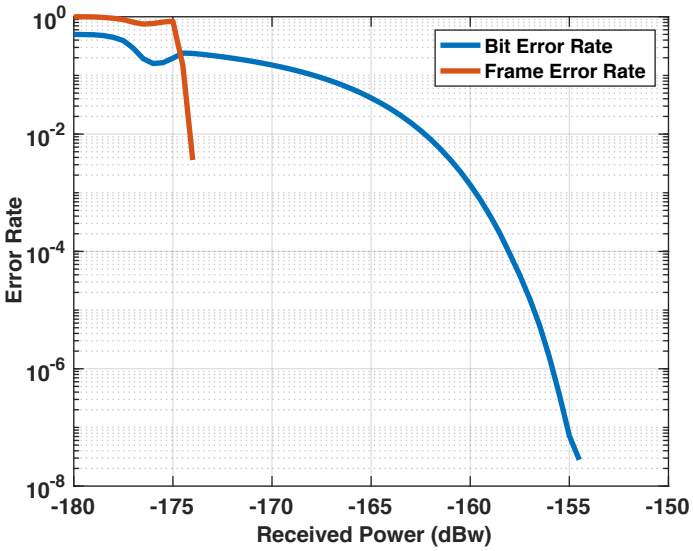

Figure 12: Results of simulating different receive powers through the software receiver. The bit-error-rates before the decoder and after the decoder were measured.

By interpolating Figure 12 using the calculated receive powers described by Equation (1), we obtained Figure 13.

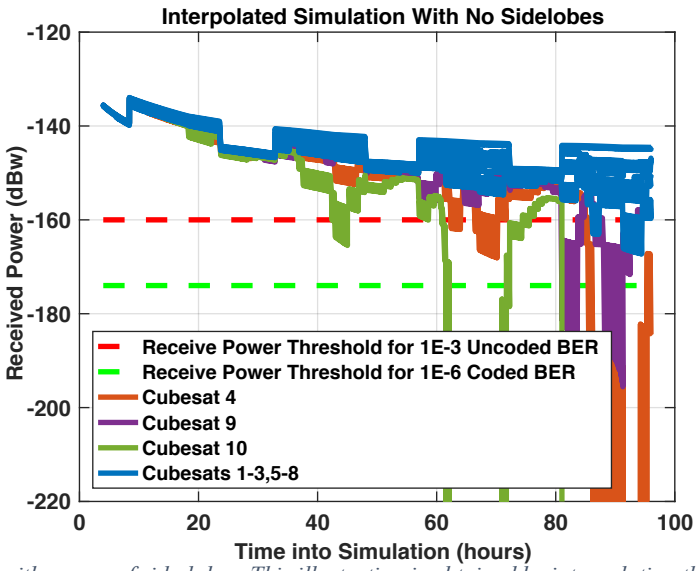

Figure 13: Simulation result with no use of side-lobes. This illustration is obtained by interpolating the curves in Figure 12 using the calculated receive power at each instant of the simulation. Observe that six out out of the ten total cubesats will experience bit-error-rates less than 1E-3 (uncoded) and 1E-6 (decoded). The simulation sampled the time-line every 5 seconds for the 96-hour simulation duration. Again, in this case, the three cubesats (4, 9, and 10) that experienced significant bit errors when exiting the main beam of the receive antenna and caused the received power of their signal to be too low for successful demodulation/decoding.

For the duration of the simulation, we found that, by just considering the main lobe of the DSN antennas, it is possible to successfully receive the data from seven out of the ten cubesats after accounting for the coding (and from all ten of the cubesats while they are all still in beam). In the next section, we examine the performance gains obtained by considering receiving some of the cubesats through the sidelobe of the antennas.

A. Impact of Antenna Sidelobes

In the previous section, we studied the impact of using only the main lobe to receive the signals from the constellation of cubesats traveling to the moon for a duration of 96 hours. In this section, we examine the performance improvement to be had by utilizing the side-lobes of the antenna as well. The antenna patterns modeled in this simulation are illustrated in Figure 4. The 34-m antenna has a beamwidth of 0.14 degrees null-to-null, while the 21-m antenna has a beamwidth of 0.24 degrees null-to-null. The result of the simulation is illustrated in Figure 14. We observe that the performance of cubesat 10 is greatly improved compared to Figure 11, especially between the hours of 60-70. This is due to the cubesat entering the first side-lobe and still obtaining enough gain to be able to close the link. Further improvement could be achieved by careful planning of which cubesat in the constellation is to be tracked so as to minimize the amount of time that the other cubesats spend directly on top of a null. Another possibility for improving performance is to reduce the code rate further so as to move the cubesat from being on the edge of reception to being easily received. This would be especially beneficial to Figure 15 discussed ahead, where the green curve would be moved slightly down by the lower code rate, allowing cubesat 10 to be received for most of 4 days. It was observed that throughout the 96 hour simulation, the cubesats did not move farther than the first side-lobe (if out of the main beam at all).

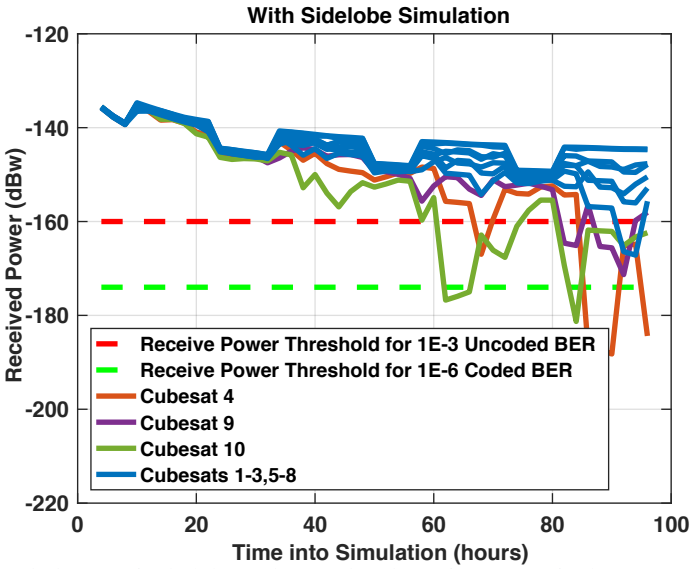

Figure 14: Simulation result with the use of side-lobes. Observe that theperformance of cubesat 10 is improved in comparison to Figure 11 especially between the hours of 60-70. The simulation sampled the time-line every 2 hours for the 96-hour simulation duration.

By interpolating Figure 12 using the calculated receive powers described by Equation (1) using the side-lobe antenna models, we obtain Figure 15. The reason why some cubesats still have some low received powers is that they lingered at the null between the main lobe and the first side-lobe simply due to the geometry of the simulation. Again, further optimization of where to point the antenna may help alleviate these issues. In general, however, the situation is much improved compared to using the main lobe only. To see this explicitly, in Figure 16, we plot the total number of lost frames throughout the simulation for each cubesat. We observe that cubesat 10's lost packets are reduced by about eight-fold by utilizing the antenna's side-lobes for cubesat reception. The failure to close the link only now occurs when the cubesat is situated at the relatively narrow null, as opposed to simply exiting the main beam.

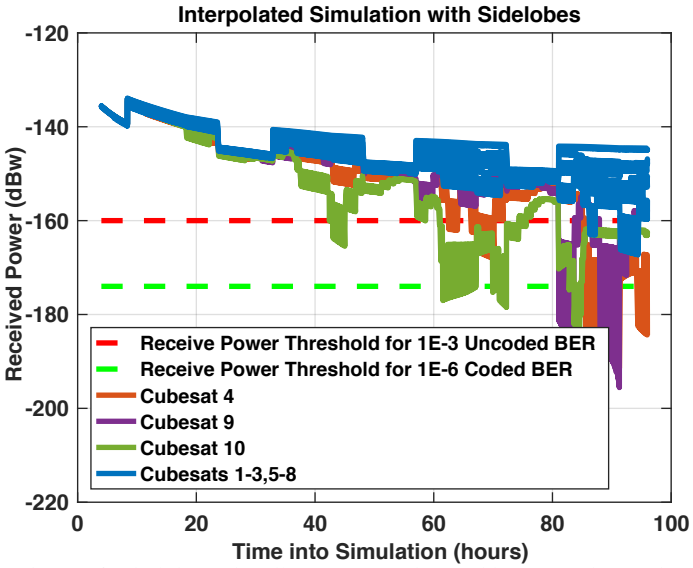

Figure 15: Simulation result with use of side-lobes. This illustration is obtained by interpolating the curves in Figure 12 using the calculated receive power at each instant of the simulation.

The reason why packet loss still occurs in the main beam plus side-lobe simulation is that the cubesat, as it transitions from the main beam to the side-lobe, will hit the null of the antenna where no energy will be detected. At a distance, if the constellation is slowly moving, the cubesat may linger around this null for a relatively long period of

time before it passes into the side-lobe or moves back into the main beam. Our simulation captures this effect, and thus some of the cubesats still experience packet loss with the main beam plus side-lobes antenna model. However, it is shown that nulls in general are not infinitely deep as modeled in this simulation, and are in fact relatively shallow[4]. This effect would actually improve the performance of the OMSPA system as it may allow even the null-lingering cubesats to have enough received power to be decoded appropriately.

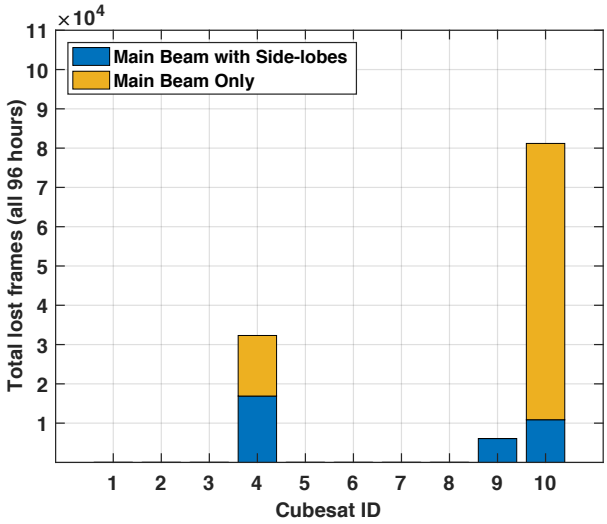

Figure 16: A graph to plot the total number of lost packets at each cubesat using two antenna models: (a) a main-beam only antenna pattern, and (b) a main-beam + side-lobes antenna pattern. It can be seen that utilizing the antenna side-lobes can greatly improve performance. Cubesats 4 and 10 achieved approximately 40% and 87% reduction in dropped frames, respectively, due to the use of the first side-lobe for receiving of the data. Cubesats 4, 9, and 10 lost less than 4% of their total transmitted frames for the duration of the 96 hour simulation when side-lobes were utilized. Other cubesats did not drop frames.

B. Impact of Antenna Size

The main differentiating feature between Morehead State University's (MSU) DSN-affiliated ground site and the other DSN sites is that MSU possesses a 21-m antenna, as opposed to the 34-m antennas available at the other sites. While the 21-m antenna delivers a lower gain compared to the 34-m antenna, it does present an advantage in OMSPA scenarios: the beam-width of the 21-m antenna (0.24 degrees null-to-null) is significantly larger than that of the 34-m meter antenna (0.14 degrees null-to-null). This presents the 21-m antenna with the advantage of being able to capture the entire cubesat simulation within its main beam for the duration of the simulation. To see this, the final constellation geometry on the antenna is illustrated in Figure 17. We observe that the entire constellation remains within the main beam of the antenna for the duration of the simulation. On the other hand, the 34-m antenna's main beam is too narrow to contain the entire constellation at the end of the 96-hour simulation. In fact, it can be seen that one cubesat happens to sit directly on top of the null for the 34-m antenna while another cubesat is in the middle of the first side-lobe.

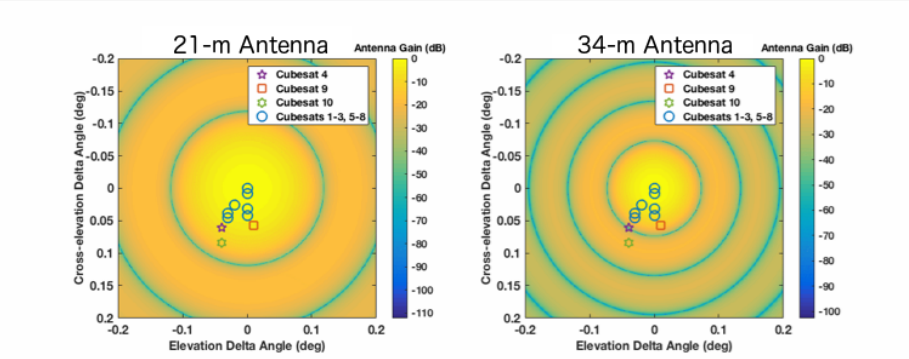

Figure 17: Constellation diagram of the geometry at the end of the simulation. A 21-m antenna can contain the entire cubesat constellation within the main beam while the 34-m antenna has cubesats on or close to its first null and a cubesat in the middle of the first side-lobe.

IX. Conclusions and Future Work

Through a simulation effort, we have demonstrated that OMSPA could be successfully used to provide for data recovery from the open-loop transmissions of multiple cubesats following their EM-1-like deployment from an upper stage rocket until execution of their TCMs. We have also shown that reliance on the antenna side-lobes at cislunar distances can significantly increase the effective antenna beam-width and associated in-beam time (though, the execution of TCMs would likely prove to be the limiting factor on in-beam time). Future plans for the OMSPA concept include an OMSPA demonstration in a multi-spacecraft environment where all spacecraft at destination are not always in-beam, as simulated in this work. Additional challenges for such a demo and associated system engineering efforts would be to find ways to speed up and automate the signal processing,,determine where best to conduct this processing given data transfer times and available ground bandwidth, and figure out how best to implement the end-to-end process in a manner that is cost-effective, for both the DSN and the potential user community.

Acknowledgments

We would like to thank NASA's Space Communications and Navigation (SCaN) office and SCaN's Program System Engineering lead at JPL, Wallace Tai, for sponsorship of this study. We also would like to thank JPL's Norman E. Lay for making the demodulation software available for this study. The research was carried out at the Jet Propulsion Laboratory, California Institute of Technology, under a contract with the National Aeronautics and Space Administration.

References

[1]Abraham, D. S., Finley, S. G., Heckman, D. P., Lay, N. E., Lush, C. M., and MacNeal, B. E., "Opportunistic MSPA Demonstration #1: Final Report," InterPlanetary Network Progress Report 42-200, pp. 1-27, Jet Propulsion Laboratory, Pasadena, California, February, 2015.

[2]Taylor, J. ed., "Deep Space Communications." JPL Deep-Space Communications and Navigation, Wiley, NJ, 2016.

[3]Lay, N., Lyubarev, M., Tkacenko, A., Srinivasan, M., Andrews, K., Finley, S., Goodhart, C., and Navarro, R., "Software Receiver Processing for Deep Space Telemetry Applications." InterPlanetary Network Progress Report 42-180, Jet Propulsion Laboratory, Pasadena, California, February, 2010.

[4]Morabito, D. D., Imbriale, W., and Keihm, S., "Observing the Moon at Microwave Frequencies Using a Large-Diameter Deep Space Network Antenna." IEEE Transactions on Antennas and Propagation, vol. 56, no. 3, March 2008, pp. 650-660.